

Unraveling the role of dipolar versus Dzyaloshinskii-Moriya interactions in stabilizing compact magnetic skyrmions

Anne Bernard-Mantel,^{1,*} Cyrill B. Muratov,² and Theresa M. Simon^{2,3}

¹*Université de Toulouse, Laboratoire de Physique et Chimie des Nano-Objets, UMR 5215 INSA, CNRS, UPS, 135 Avenue de Rangueil, F-31077 Toulouse Cedex 4, France*

²*Department of Mathematical Sciences, New Jersey Institute of Technology, Newark, New Jersey 07102, USA*

³*Institute for Applied Mathematics, University of Bonn, Endenicher Allee 60, 53115 Bonn, Germany*



(Received 4 August 2019; revised manuscript received 14 October 2019; published 14 January 2020)

We present a theoretical study of compact magnetic skyrmions in ferromagnetic films with perpendicular magnetic anisotropy that accounts for the full stray field energy in the thin film and low interfacial Dzyaloshinskii-Moriya interaction (DMI) regime. In this regime, the skyrmion profile is close to a Belavin-Polyakov profile, which yields analytical expressions for the equilibrium skyrmion radius and energy. The obtained formulas provide a clear identification of DMI and long-range dipolar interaction as two physical mechanisms determining skyrmion size and stability.

DOI: [10.1103/PhysRevB.101.045416](https://doi.org/10.1103/PhysRevB.101.045416)

I. INTRODUCTION

Magnetic skyrmions are a prime example of topologically nontrivial spin textures observed in a variety of magnetic materials. Their nucleation and annihilation in an otherwise uniformly magnetized ferromagnet is enabled by the discrete nature of matter [1–4]. Magnetic skyrmions emerge when the exchange and anisotropy energies promoting parallel alignment of spins in a ferromagnet enter in competition with energies favoring noncollinear alignment of spins such as the Dzyaloshinskii-Moriya interaction (DMI) [5,6], the long-range dipolar interaction [7,8], or higher order exchange interactions [9–11]. In particular, DMI is at the heart of a large number of magnetic skyrmion observations in recent years. This antisymmetric exchange interaction is related to the lack of structural inversion symmetry and is present in a variety of bulk chiral magnets [12–16]. Interfacial DMI induced by the symmetry breaking in ferromagnetic heterostructures with asymmetric interfaces [17–19] also leads to the formation of skyrmions in thin ferromagnetic layers [1,20,21] and multilayers [22]. Another classical energy term known to favor noncollinear spin alignment in ferromagnets is the dipolar energy, also called stray field or demagnetizing energy [23]. A manifestation of the long-range nature of this energy in thin films with perpendicular magnetic anisotropy is the appearance of micron-sized magnetic bubble domains [8,24–26]. The equilibrium shape and size of these domains is determined by the balance between the long-range dipolar interaction and the energy cost of the bubble related to the domain wall energy and the Zeeman energy [27].

The orthodox theory of skyrmions in ultrathin ferromagnetic layers with interfacial DMI relies on a model that accounts for the dipolar interaction through an effective

anisotropy term, neglecting long-range effects [9,28]. At the same time, in single ferromagnetic layers with interfacial DMI, large chiral skyrmions, also called skyrmionic bubbles, have been observed [29–33], suggesting a nontrivial interplay between DMI and long-range dipolar effects. The competition between these two energies also leads to the formation of skyrmions exhibiting spin rotations with intermediate angles between Néel and Bloch [34–36], a phenomenon also present in domain walls [37]. In addition, there is a growing body of theoretical evidence that points to a need to take into account the long-range dipolar energy in the models describing magnetic skyrmions [27,34,38,39]. In particular, Büttner *et al.* [34] used a 360°-wall ansatz [40] to numerically calculate the skyrmion equilibrium radius and energy as functions of the material parameters for intermediate thicknesses, focusing on room-temperature stable skyrmions and predicting the existence of room temperature skyrmions stabilized solely by the stray field.

The above considerations put into question the validity of the commonly used assumption that the contribution of the long-range dipolar interaction is negligible. Another open question is whether there exists a size difference between the skyrmions stabilized by the DMI and those stabilized by the stray field [27,34,38,39]. In this paper, we address these questions using an ansatz-free analysis of a micromagnetic model that is valid for sufficiently small film thicknesses. We provide explicit analytical expressions for the skyrmion radius, rotation angle, and energy valid in the low DMI and thickness regime, taking into account the long-range dipolar energy contribution. We obtain a prediction for the critical DMI value at which the skyrmion character changes from pure Néel to a mixed Néel-Bloch type. These findings are corroborated by micromagnetic simulations. Our rigorous treatment of the stray field contribution sheds light on the necessity to tune both the magnetic layer thickness and the DMI constant to optimize the skyrmion size and stability for applications.

*bernandm@insa-toulouse.fr

II. MODEL

We consider a ferromagnetic thin film with perpendicular magnetic anisotropy (PMA) and infinite extent in the plane. The film is assumed to be sufficiently thin in order for the magnetization vector \mathbf{m} to be constant in the direction normal to the film plane. Under these conditions, the micromagnetic energy [23] reduces to [41–43]

$$\begin{aligned}
 E(\mathbf{m}) = & \int_{\mathbb{R}^2} (|\nabla \mathbf{m}|^2 + (Q - 1)|\mathbf{m}_\perp|^2) d^2 r \\
 & + \kappa \int_{\mathbb{R}^2} (m_\parallel \nabla \cdot \mathbf{m}_\perp - \mathbf{m}_\perp \cdot \nabla m_\parallel) d^2 r \\
 & - \frac{\delta}{8\pi} \int_{\mathbb{R}^2} \int_{\mathbb{R}^2} \frac{(m_\parallel(\mathbf{r}) - m_\parallel(\mathbf{r}'))^2}{|\mathbf{r} - \mathbf{r}'|^3} d^2 r d^2 r' \\
 & + \frac{\delta}{4\pi} \int_{\mathbb{R}^2} \int_{\mathbb{R}^2} \frac{\nabla \cdot \mathbf{m}_\perp(\mathbf{r}) \nabla \cdot \mathbf{m}_\perp(\mathbf{r}')}{|\mathbf{r} - \mathbf{r}'|} d^2 r d^2 r'. \quad (1)
 \end{aligned}$$

Here E is measured in the units of Ad , where A is the exchange stiffness and d is the film thickness, lengths are measured in the units of the exchange length $\ell_{\text{ex}} = \sqrt{2A/(\mu_0 M_s^2)}$, M_s is the saturation magnetization, and $\delta = d/\ell_{\text{ex}} \lesssim 1$ is the dimensionless film thickness (for further details, see Ref. [44]). Furthermore, in Eq. (1) we set $\mathbf{m} = (\mathbf{m}_\perp, m_\parallel)$, where $\mathbf{m}_\perp \in \mathbb{R}^2$ and $m_\parallel \in \mathbb{R}$ are the respective in-plane and out-of-plane components of \mathbf{m} , and introduced the dimensionless quality factor $Q = K_u/K_d$, where K_u is the magnetocrystalline anisotropy constant, $K_d = \frac{1}{2}\mu_0 M_s^2$, and the dimensionless DMI strength $\kappa = D/\sqrt{AK_d}$. The first three energy terms are local and represent, respectively, the exchange energy, the effective anisotropy energy, which corresponds to the magnetocrystalline energy renormalized to take into account the local stray field contribution, and the DMI energy. The last two terms correspond to the long-range part of the dipolar energy, which splits into two contributions. The first contribution is due to the out-of-plane component of \mathbf{m} and accounts for surface charges at the top and bottom interfaces of the film. The second energy term corresponds to volume charges and is due to the in-plane divergence of the magnetization.

III. RESULTS AND DISCUSSION

A. Definition of a skyrmion

Magnetic skyrmions were originally predicted to exist using a fully local micromagnetic model that is obtained from Eq. (1) by setting $\delta = 0$ [5,6,45]. Within this model [46,47], the ground state for PMA materials ($Q > 1$) and sufficiently small values of $|\kappa|$ is the monodomain state $\mathbf{m} = \pm \hat{\mathbf{z}}$, where $\hat{\mathbf{z}}$ is the unit normal vector to the film plane (the xy plane) [41,45]. Therefore, one should identify magnetic skyrmions with metastable magnetization configurations that locally minimize the energy in Eq. (1). In addition, skyrmions possess a nonzero topological charge $q \in \mathbb{Z}$ defined as [48–50]

$$q(\mathbf{m}) = \frac{1}{4\pi} \int_{\mathbb{R}^2} \mathbf{m} \cdot \left(\frac{\partial \mathbf{m}}{\partial x} \times \frac{\partial \mathbf{m}}{\partial y} \right) dx dy, \quad (2)$$

provided $\lim_{|\mathbf{r}| \rightarrow \infty} \mathbf{m}(\mathbf{r}) = -\hat{\mathbf{z}}$ in order to fix the sign convention so that $q = +1$ for either the Néel or Bloch skyrmion profiles. In a fully local micromagnetic model with bulk DMI

and no anisotropy term, Melcher [51] studied the existence of minimizers among nontrivial topological sectors in the presence of a sufficiently strong Zeeman term. He found that in this class the energy is globally minimized by a configuration with $q = +1$ (in our convention) and identified this energy-minimizing magnetization configuration with a magnetic skyrmion.

In contrast, in the absence of an applied magnetic field and in the presence of long-range dipolar interaction, the monodomain state is never the ground state in an extended ferromagnetic film [42,52]. This can be seen by noting that the energy in Eq. (1) with $Q > 1$ and $\delta > 0$ goes to negative infinity for configurations consisting of a growing bubble domain in which the $\mathbf{m} = +\hat{\mathbf{z}}$ core is separated from the $\mathbf{m} = -\hat{\mathbf{z}}$ background by a Bloch or Néel wall, depending on the magnitude of $|\kappa|$, and which carry the topological charge $q = +1$ [27,42]. Thus, it is not possible to carry out the analysis of Ref. [51] to establish existence of skyrmion profiles via direct energy minimization without introducing further restrictions on the admissible configurations distinguishing compact magnetic skyrmions from skyrmionic bubbles.

In the present work, we assign a mathematical meaning to the notion of compact magnetic skyrmion by defining a class of admissible configurations in which the topological charge is fixed to $q = +1$ and the exchange energy cannot exceed twice the topological lower bound, i.e., twice the exchange energy of the Belavin-Polyakov profile [27,34,53]. Within this class, we establish the existence of compact skyrmions as minimizers of the energy in Eq. (1) for an explicit range of the parameters.

Theorem 1. Let $Q > 1$, $\delta > 0$ and $\kappa \in \mathbb{R}$ be such that

$$(2|\kappa| + \delta)^2 < 2(Q - 1). \quad (3)$$

Then there exists a minimizer of E among all \mathbf{m} such that $q(\mathbf{m}) = +1$, $\int_{\mathbb{R}^2} |\nabla \mathbf{m}|^2 d^2 r < 16\pi$, and $\mathbf{m}(\mathbf{r}) \rightarrow -\hat{\mathbf{z}}$ as $|\mathbf{r}| \rightarrow \infty$.

A more precise statement and a sketch of the proof of this result may be found in the Supplemental Material [44]. In the following, we always refer to the minimizers in the above theorem as *skyrmion solutions*. We note that Eq. (3) is only a sufficient condition for their existence.

B. Skyrmion solutions in the low $|\kappa|$ and δ regime

Once existence of a compact skyrmion solution is established, we proceed with an asymptotic analysis of the skyrmion profile at low values of $|\kappa|$ and δ (for a fully rigorous treatment, see Ref. [54]). It is known that in a model with exchange energy alone the minimizer is given explicitly by all rigid in-plane rotations, dilations, and translations of the Belavin-Polyakov profile [53]. It can be expected that in the limit where additional energy terms appear as perturbations (low $|\kappa|$ and δ) of the dominating exchange energy, skyrmions retain the Belavin-Polyakov profile [10]. This has been demonstrated recently via a formal asymptotic analysis of radial skyrmion solutions in the local model with bulk DMI in the limit of vanishing DMI constant [55]. In the full model given in Eq. (1), we were able to prove [54] that as $\kappa, \delta \rightarrow 0$ the energy-minimizing profile \mathbf{m} converges to a

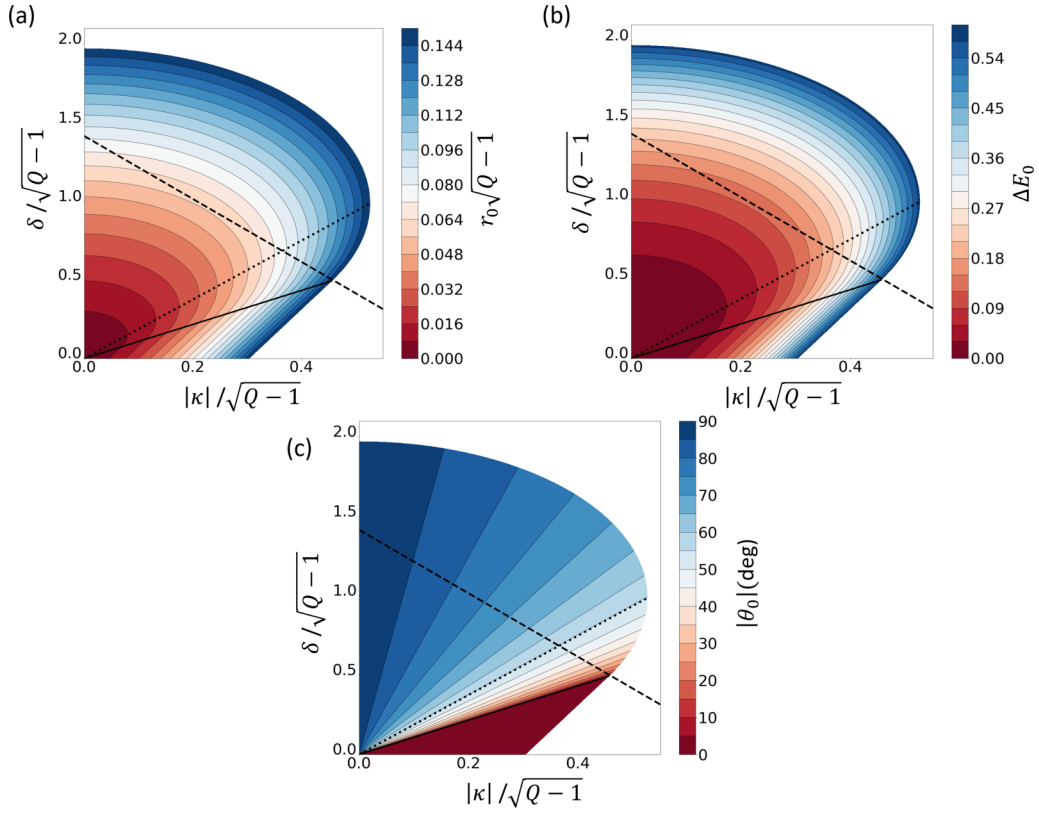


FIG. 1. Dependences of the skyrmion characteristics on the parameters obtained from the asymptotic analysis for $|\kappa|, \delta \ll \sqrt{Q-1}$: (a) the dimensionless skyrmion radius r_0 from Eq. (6); (b) the skyrmion collapse energy barrier ΔE_0 from Eq. (8); and (c) the rotation angle $|\theta_0|$ from Eq. (5). The solid line shows the transition from Néel to mixed Néel-Bloch skyrmions governed by Eq. (9). The dashed line corresponds to the boundary of the region defined in Eq. (3) in which existence of skyrmion solutions is guaranteed. The dotted line shows the parameters at which the skyrmion radius achieves its minimum value as a function of δ according to Eq. (11).

Belavin-Polyakov profile \mathbf{m}_0 given by

$$\mathbf{m}_0(\mathbf{r}) = \left(-\frac{2r_0 R_{\theta_0} \mathbf{r}}{|\mathbf{r}|^2 + r_0^2}, \frac{r_0^2 - |\mathbf{r}|^2}{r_0^2 + |\mathbf{r}|^2} \right) \mathbf{r} \in \mathbb{R}^2, \quad (4)$$

where R_{θ_0} is the 2×2 matrix of in-plane rotations by angle

$$\theta_0 = \begin{cases} 0 & \text{if } \kappa \geq \frac{3\pi^2}{32} \delta, \\ -\pi & \text{if } \kappa \leq -\frac{3\pi^2}{32} \delta, \\ \pm \arccos\left(\frac{32\kappa}{3\pi^2 \delta}\right) & \text{else,} \end{cases} \quad (5)$$

and the dimensionless skyrmion radius is asymptotically

$$r_0 \simeq \frac{1}{16\pi \sqrt{Q-1}} \frac{\bar{\varepsilon}(\kappa, \delta, Q)}{|\ln(\beta \bar{\varepsilon}(\kappa, \delta, Q))|}, \quad (6)$$

for $\beta \bar{\varepsilon} \ll 1$ with $\beta \approx 0.04816$ and

$$\bar{\varepsilon}(\kappa, \delta, Q) = \frac{1}{\sqrt{Q-1}} \begin{cases} 8\pi |\kappa| - \frac{\pi^3}{4} \delta & \text{if } |\kappa| \geq \frac{3\pi^2}{32} \delta, \\ \frac{128\kappa^2}{3\pi \delta} + \frac{\pi^3}{8} \delta & \text{else.} \end{cases} \quad (7)$$

The above expressions may be obtained by considering a suitably truncated magnetization profile in the form of Eq. (4), optimizing in θ_0 and r_0 , and expanding the obtained expressions in the leading order of δ and $|\kappa|$ (see Ref. [44] for more details). Our analysis also yields the following asymptotic expression for the skyrmion energy:

$$E_0 \simeq 8\pi - \frac{\bar{\varepsilon}^2(\kappa, \delta, Q)}{32\pi |\ln(\beta \bar{\varepsilon}(\kappa, \delta, Q))|}. \quad (8)$$

The associated skyrmion collapse energy barrier $\Delta E_0 = 8\pi - E_0$ gives an indication of the skyrmion stability as it represents the energy necessary to suppress the skyrmion via compression [3,27,34]. The solution described in Eqs. (4)–(8) is asymptotically exact to the leading order for $|\kappa| \ll \sqrt{Q-1}$ and $\delta \ll \sqrt{Q-1}$, but in practice remains at least qualitatively correct also up to $\kappa \sim \sqrt{Q-1}$ and $\delta \sim \sqrt{Q-1}$. Nevertheless, to avoid artifacts from the predictions of our formulas outside their range of validity, we somewhat arbitrarily restrict the considered parameters to those for which $\beta \bar{\varepsilon}(\kappa, \delta, Q) \leq e^{-1}$, ensuring $|\ln(\beta \bar{\varepsilon}(\kappa, \delta, Q))| \geq 1$.

C. Asymptotic properties of skyrmion solutions

The dependences of the dimensionless skyrmion radius r_0 , the collapse energy ΔE_0 , and the rotation angle θ_0 on the model parameters obtained from the asymptotic analysis of Sec. III B are presented in Fig. 1. The first important characteristic of the solution is the existence of a minimum or threshold $|\kappa|$ value

$$|\kappa|_{\text{sky}}^{\text{thresh}} = \frac{3\pi^2}{32} \delta, \quad (9)$$

above which pure Néel skyrmions ($\theta_0 = 0$ or $\theta_0 = -\pi$, depending on the sign of κ) are obtained and below which skyrmions are characterized by a nonzero rotation angle θ_0 . This angle tends to $\pm\pi/2$, corresponding to pure Bloch

skyrmions when $\kappa \rightarrow 0$. It is a direct consequence of the competition between long-range dipolar interaction, which favors a Bloch rotation, and interfacial DMI, which favors a Néel rotation. Note that a similar threshold is observed in the case of straight domain walls [37,56]:

$$|\kappa|_{\text{wall}}^{\text{thresh}} = \frac{4 \ln 2}{\pi^2} \delta. \quad (10)$$

Thus, a larger DMI is necessary to obtain a pure Néel skyrmion as compared to the case of a one-dimensional (1D) Néel wall, as can be seen from the factor of ≈ 3 difference between the values of $|\kappa|_{\text{sky}}^{\text{thresh}}$ and $|\kappa|_{\text{wall}}^{\text{thresh}}$. This is an indication that dipolar effects play a stronger role for skyrmions compared to domain walls.

The second characteristic associated with the interplay between DMI and the dipolar interaction that is visible in Figs. 1(a) and 1(b) is the nonmonotone dependence of the dimensionless skyrmion radius r_0 and collapse energy ΔE_0 on δ for Q and κ fixed. For δ below the critical value where skyrmions are of Néel character, the skyrmion radius decreases with increasing δ , while for large enough δ , in the regime with nonzero θ_0 , the radius increases with δ . As can be seen from Eq. (6), the skyrmion radius reaches its minimum at $\delta = \delta_{\text{opt}}$, where

$$\delta_{\text{opt}} = \frac{32|\kappa|}{\pi^2\sqrt{3}}. \quad (11)$$

This observation is of importance for applications, as the thickness of the film is the parameter which is the most easy to tune experimentally for a thin film in order to optimize the skyrmion size and stability. Interestingly, at $\delta = \delta_{\text{opt}}$ the rotation angle θ_0 attains a universal value of $\theta_0^{\text{opt}} = \pm \arccos(\text{sgn}(\kappa)/\sqrt{3})$, i.e., $\theta_0^{\text{opt}} \approx \pm 54.74^\circ$ for $\kappa > 0$ or $\theta_0^{\text{opt}} \approx \pm 125.3^\circ$ for $\kappa < 0$.

The third important result illustrated in Fig. 1 is the existence of skyrmions stabilized solely by the long-range dipolar interaction for $\kappa = 0$. Such dipolar skyrmions possess a pure Bloch character ($\theta_0 = \pm\pi/2$), with volume charges not contributing to the energy. We observe in Fig. 1(a) that, starting from $\kappa = 0$ and following a skyrmion solution of fixed radius while decreasing δ , one goes continuously from a Bloch skyrmion at $\kappa = 0$ to a Néel skyrmion at $\delta = 0$. Consequently, skyrmions stabilized by DMI and stray field cannot be distinguished by their radius.

D. Phase diagram

To complete our description, we locate the skyrmion solutions on a phase diagram (see Fig. 2). For that purpose, we fix a representative set of parameters: exchange constant $A = 20$ pJ/m, film thickness $d = 1$ nm, and DMI constant $D = 0.3$ mJ/m², and vary the saturation magnetization M_s and magnetocrystalline anisotropy constant K_u over a wide range. The solid black line represents the threshold at which the magnetization reorientation transition between in-plane and out-of-plane occurs ($Q = 1$, i.e., for $K_u = K_d$). In the dark blue region above this line, the magnetization prefers to lie in the film plane, and no compact skyrmion solutions exist in an infinite film. Below this line, the easy axis is perpendicular to the film plane. In the zone represented in

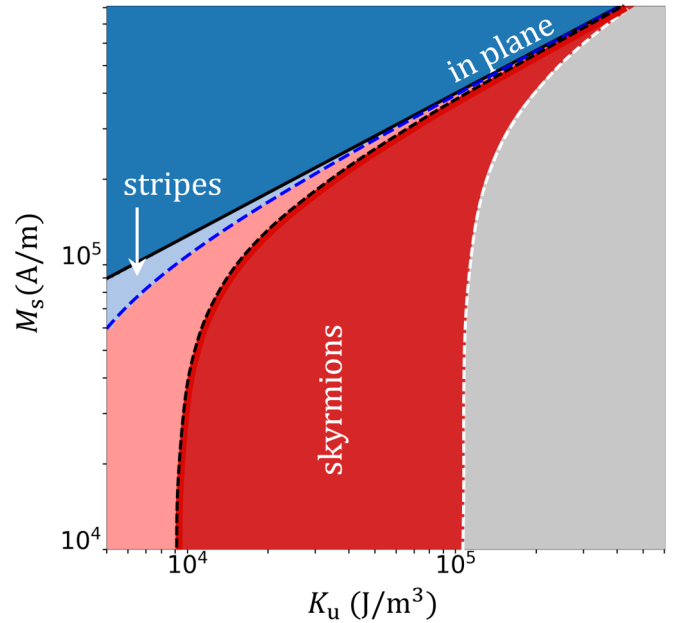


FIG. 2. Skyrmion phase diagram for $A = 20$ pJ/m, $D = 0.3$ mJ/m², and $d = 1$ nm. The dark red zone is the domain of existence of our skyrmion solutions (see Sec. III D for a complete description of the different zones and lines).

light blue, the domain wall energy density defined as $\sigma_{\text{wall}} = 4\sqrt{A(K_u - K_d)} - \pi D$ is negative. Here, the expected ground state of the thin film is the helicoidal state [58], and isolated compact skyrmions do not exist in the absence of an applied magnetic field [1]. Below the dashed blue line corresponding to $K_u^{\text{crit}} = \frac{\pi^2 D^2}{16A} + K_d$, the ferromagnetic ground state is restored, the domain wall energy becomes positive again, and compact skyrmions may exist as metastable states. In the light red region, the existence of compact skyrmion solutions as metastable state is not guaranteed. Indeed, in this region close to the transition to the helicoidal state, skyrmions may be subject to elliptical instabilities favored by both the DMI and the long-range dipolar interaction [23,59]. The dark red zone represents the domain of existence of our skyrmion solutions. It is delimited on one side by a dashed black line, which represents the boundary of the region defined by Eq. (3), below which we have existence of a compact skyrmion. When the anisotropy is further increased (or M_s is decreased), the limit of validity of our 2D thin film model is reached as the skyrmion radius becomes of the order of the film thickness. The white dashed line represents the line at which $r_{\text{sky}} = d$ as a guide to the eye. We point out that below this line skyrmion solutions may exist and develop z dependence [35,39]. Further below this line, the continuum micromagnetic model is no longer valid, as the skyrmion radius becomes of the order of the interatomic spacing.

E. Application to specific examples for low and intermediate D values

In this section, we apply our compact skyrmion results to the case of *ferrimagnetic* materials, i.e., materials with low M_s and K_u values (e.g., GdCo [60]). These conditions

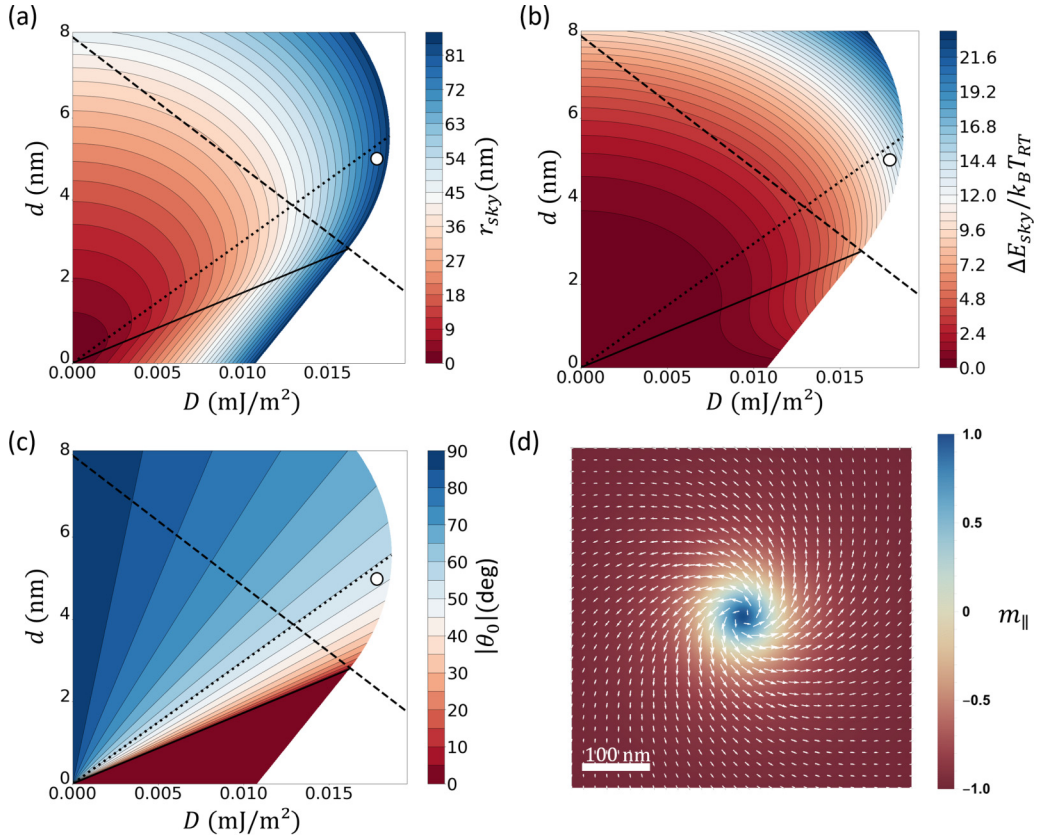


FIG. 3. Dependences of the skyrmion characteristics in the low-DMI regime. The parameters are $A = 20$ pJ/m, $M_s = 10^5$ A/m, and $K_u = 6346$ J/m³ corresponding to $Q = 1.01$. (a) The skyrmion radius r_{sky} . (b) The normalized skyrmion collapse energy barrier $\Delta E_{\text{sky}}/(k_B T_{293\text{K}})$. (c) The rotation angle $|\theta_0|$. (d) The skyrmion profile obtained numerically for $d = 5$ nm and $D = 0.018$ mJ/m², corresponding to the white dots in panels (a)–(c), using MuMax3 [57] on a 4096×4096 nm² square domain subject to periodic boundary conditions, with the mesh size of $4 \times 4 \times 5$ nm³. The image in panel (d) is constructed by superimposing the in-plane magnetization \mathbf{m}_\perp represented with arrows and the out-of-plane magnetization m_\parallel represented by a color map. The lines in panels (a)–(c) are the same as in Fig. 1.

favor the observation of skyrmions in the absence of an applied magnetic field, as discussed in the previous section. An observation of room-temperature zero-field skyrmions in this material was recently reported [60].

In Fig. 3, we present the case of low D values for which the transition from pure Néel to pure Bloch skyrmion appears, as seen in Fig. 3(c). For comparison, we carried out micromagnetic simulations for the parameters corresponding to the white dots in Fig. 3(a)–3(c) (see figure caption for details). From the simulations, we obtain a skyrmion with a rotation angle $\theta_0 \simeq 46^\circ$ and a radius $r_{\text{sky}} \simeq 52$ nm, versus $\theta_0 \simeq 52^\circ$ and $r_{\text{sky}} \simeq 80$ nm from the analytical formulas. This confirms the transition from purely Néel, to intermediate Néel-Bloch rotation angle, predicted by our analysis at lower thicknesses compared to 1D walls as discussed in Sec. III C. Indeed, for 1D walls, a purely Néel character is expected up to thicknesses of ≈ 10 nm. This validates the increased importance of dipolar interaction in the case of compact skyrmions predicted by our theory compared to 1D walls. Figure 3(b) shows the skyrmion collapse energy barrier $\Delta E_{\text{sky}} = \Delta E_0 A d$ normalized by the room temperature thermal energy $k_B T_{293\text{K}}$. The collapse energy barrier ΔE_{sky} obtained by our analysis is $13 k_B T_{293\text{K}}$, compared to $15.5 k_B T_{293\text{K}}$ from the micromagnetic simulations. We observe that in the low D regime the collapse barrier increase with film thickness.

This consideration justifies the choice of systems with bulk out-of-plane anisotropy (like the ferrimagnetic alloy GdCo) or multilayers [e.g., (Pt/Co/Ir)_n] to optimize skyrmion lifetime, since it allows one to increase the film thickness (or effective thickness) without losing the out-of-plane anisotropy, as would be the case for single ferromagnetic layers with surface-induced anisotropy alone [22,60].

In Fig. 4, we present the results for an intermediate DMI range where the D values are an order of magnitude larger than those in Fig. 3. We use the same parameters as in Fig. 3, except $K_u = 1.26 \times 10^4$ J/m³ corresponding to $Q = 2$. All the solutions in Fig. 4 are the iconic Néel skyrmions with $\lesssim 10$ nm radii that grow with an increase of the DMI strength [see Fig. 4(a)]. The skyrmion collapse barrier can be heightened by either increasing the film thickness or the DMI strength [see Fig. 4(b)]. In the low thickness regime, the decrease of the collapse barrier with the film thickness is due to the dimensional scale factor of Ad . The same phenomenon is at the origin of the short skyrmion lifetime (≈ 1 s) observed experimentally at low temperature in ferromagnetic monolayers [1], despite a large DMI constant [61].

We observe in Fig. 4(b) that the collapse energy barrier of ≈ 8 nm radius skyrmions reaches $22 k_B T_{293\text{K}}$, which corresponds to a lifetime of a few seconds, considering the Néel-Brown model with the attempt frequency $\nu = 10^9$ s⁻¹.

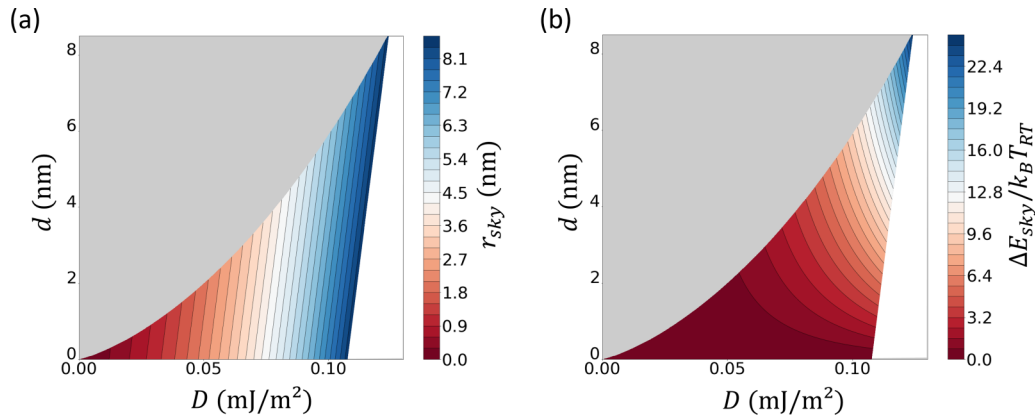


FIG. 4. Dependences of the skyrmion characteristics in the intermediate DMI regime. The parameters are $A = 20$ pJ/m, $M_s = 10^5$ A/m, and $K_u = 1.26 \times 10^4$ J/m³ corresponding to $Q = 2$. (a) The skyrmion radius r_{sky} . (b) The normalized skyrmion collapse energy barrier $\Delta E_{\text{sky}}/(k_B T_{293K})$. The gray zone corresponds to the region where $r_{\text{sky}} < d$.

At fixed thickness d , the skyrmion radius decreases with the DMI strength, and the limit of validity of our thin film model is reached as the skyrmion radius becomes of the same order as the film thickness. In this regime, 3D models and full 3D micromagnetic simulations will be needed to take into account the long-range dipolar effects.

IV. SUMMARY

We have used rigorous mathematical analysis to develop a skyrmion theory that takes into account the full dipolar energy in the thin film regime and provides analytical formulas for compact skyrmion radius, rotation angle and energy. While long-range interactions are often assumed to have a negligible impact on skyrmions in this regime, we demonstrate that the DMI threshold at which a compact skyrmion loses its Néel character is a factor of ≈ 3 higher than that for a 1D wall. A reorientation of the skyrmion rotation angle from Néel to intermediate Néel-Bloch angles is predicted as the

layer thickness is increased in the low DMI regime, which is confirmed by micromagnetic simulations. The estimation of this reorientation thickness is important for applications as the skyrmion angle affects its current-induced dynamics [62].

ACKNOWLEDGMENTS

A.B.-M. wishes to acknowledge support from DARPA TEE program through Grant MIPR No. HR0011831554. The work of C.B.M. and T.M.S. was supported, in part, by NSF via Grants No. DMS-1614948 and No. DMS-1908709. C.B.M. would also like to acknowledge support by CNRS via EUR Grant NanoX No. ANR-17-EURE-0009 in the framework of the “Programme des Investissements d’Avenir” and LPCNO, INSA, Toulouse, France, for its hospitality. This work benefited from access to the HPC resources of CALMIP supercomputing center under the Allocation No. 2019-19011. The authors also acknowledge the hospitality of Erwin Schrödinger International Institute for Mathematics and Physics.

-
- [1] N. Romming, C. Hanneken, M. Menzel, J. E. Bickel, B. Wolter, K. von Bergmann, A. Kubetzka, and R. Wiesendanger, *Science* **341**, 636 (2013).
- [2] A. D. Verga, *Phys. Rev. B* **90**, 174428 (2014).
- [3] D. Cortés-Ortuño, W. Wang, M. Beg, R. A. Pepper, M.-A. Bisotti, R. Carey, M. Vousden, T. Kluyver, O. Hovorka, and H. Fangohr, *Sci. Rep.* **7**, 4060 (2017).
- [4] J. Hagemester, N. Romming, K. von Bergmann, E. Y. Vedmedenko, and R. Wiesendanger, *Nat. Commun.* **6**, 8455 (2015).
- [5] A. N. Bogdanov and D. A. Yablonskii, *JETP* **68**, 101 (1989).
- [6] A. N. Bogdanov, M. V. Kudinov, and D. A. Yablonskii, *Sov. Phys.-Solid State* **31**, 1707 (1989).
- [7] X. Z. Yu, K. Shibata, W. Koshihase, Y. Tokunaga, Y. Kaneko, T. Nagai, K. Kimoto, Y. Taguchi, N. Nagaosa, and Y. Tokura, *Phys. Rev. B* **93**, 134417 (2016).
- [8] S. A. Montoya, S. Couture, J. J. Chess, J. C. T. Lee, N. Kent, D. Henze, S. K. Sinha, M.-Y. Im, S. D. Kevan, P. Fischer *et al.*, *Phys. Rev. B* **95**, 024415 (2017).
- [9] B. Ivanov, V. Stephanovich, and A. Zhmudskii, *J. Magn. Magn. Mater.* **88**, 116 (1990).
- [10] A. Abanov and V. L. Pokrovsky, *Phys. Rev. B* **58**, R8889 (1998).
- [11] T. Okubo, S. Chung, and H. Kawamura, *Phys. Rev. Lett.* **108**, 017206 (2012).
- [12] S. Mühlbauer, B. Binz, F. Jonietz, C. Pfleiderer, A. Rosch, A. Neubauer, R. Georgii, and P. Böni, *Science* **323**, 915 (2009).
- [13] X. Z. Yu, Y. Onose, N. Kanazawa, J. H. Park, J. H. Han, Y. Matsui, N. Nagaosa, and Y. Tokura, *Nature (London)* **465**, 901 (2010).
- [14] Y. Tokunaga, X. Z. Yu, J. S. White, H. M. Ronnow, D. Morikawa, Y. Taguchi, and Y. Tokura, *Nat. Commun.* **6**, 7638 (2015).
- [15] I. Kézsmárki, S. Bordács, P. Milde, E. Neuber, L. M. Eng, J. S. White, H. M. Ronnow, C. D. Dewhurst, M. Mochizuki, K. Yanai *et al.*, *Nat. Mat.* **14**, 1116 (2015).
- [16] S. Seki, X. Z. Yu, S. Ishiwata, and Y. Tokura, *Science* **336**, 198 (2012).

- [17] M. Bode, M. Heide, K. von Bergmann, P. Ferriani, S. Heinze, G. Bihlmayer, A. Kubetzka, O. Pietzsch, S. Blügel, and R. Wiesendanger, *Nature (London)* **447**, 190 (2007).
- [18] M. Heide, G. Bihlmayer, and S. Blügel, *Phys. B (Amsterdam, Neth.)* **404**, 2678 (2009).
- [19] H. Yang, A. Thiaville, S. Rohart, A. Fert, and M. Chshiev, *Phys. Rev. Lett.* **115**, 267210 (2015).
- [20] S. Heinze, K. von Bergmann, M. Menzel, J. Brede, A. Kubetzka, R. Wiesendanger, G. Bihlmayer, and S. Blügel, *Nat. Phys.* **7**, 713 (2011).
- [21] M. Hervé, B. Dupé, R. Lopes, M. Böttcher, M. D. Martins, T. Balashov, L. Gerhard, J. Sinova, and W. Wulfhekel, *Nat. Commun.* **9**, 1015 (2018).
- [22] C. Moreau-Luchaire, C. Moutafis, N. Reyren, J. Sampaio, N. Van Horne, C. A. F. Vaz, K. Bouzehouane, K. Garcia, C. Deranlot, P. Warnicke *et al.*, *Nat. Nanotechnol.* **11**, 444 (2016).
- [23] A. Hubert and R. Schäfer, *Magnetic Domains* (Springer, Berlin, 1998).
- [24] C. Kooy and U. Enz, *Philips Res. Rep.* **15**, 7 (1960).
- [25] A. Bobeck, *Bell System. Tech. J.* **46**, 1901 (1967).
- [26] P. Chaudhari, J. J. Cuomo, and R. J. Gambino, *Appl. Phys. Lett.* **22**, 337 (1973).
- [27] A. Bernard-Mantel, L. Camosi, A. Wartelle, N. Rougemaille, M. Darques, and L. Ranno, *SciPost. Phys.* **4**, 027 (2018).
- [28] S. Rohart and A. Thiaville, *Phys. Rev. B* **88**, 184422 (2013).
- [29] W. Jiang, P. Upadhyaya, W. Zhang, G. Yu, M. B. Jungfleisch, F. Y. Fradin, J. E. Pearson, Y. Tserkovnyak, K. L. Wang, O. Heinonen *et al.*, *Science* **349**, 283 (2015).
- [30] F. Büttner, C. Moutafis, M. Schneider, B. Kruger, C. M. Gunther, J. Geilhufe, C. v. Korff Schmising, J. Mohanty, B. Pfau, S. Schaffert *et al.*, *Nat. Phys.* **11**, 225 (2015).
- [31] S. Woo, K. Litzius, B. Kruger, M.-Y. Im, L. Caretta, K. Richter, M. Mann, A. Krone, R. M. Reeve, M. Weigand *et al.*, *Nat. Mat.* **15**, 501 (2016).
- [32] G. Yu, P. Upadhyaya, X. Li, W. Li, W. K. Kim, Y. Fan, K. L. Wong, Y. Tserkovnyak, P. K. Amiri, and K. L. Wang, *Nano Lett.* **16**, 1981 (2016).
- [33] M. Schott, A. Bernard-Mantel, L. Ranno, S. Pizzini, J. Vogel, H. Béa, C. Baraduc, S. Auffret, G. Gaudin, and D. Givord, *Nano Lett.* **17**, 3006 (2017).
- [34] F. Büttner, I. Lemesch, and G. S. D. Beach, *Sci. Rep.* **8**, 4464 (2018).
- [35] W. Legrand, J.-Y. Chauleau, D. Maccariello, N. Reyren, S. Collin, K. Bouzehouane, N. Jaouen, V. Cros, and A. Fert, *Sci. Adv.* **4**, eaat0415 (2018).
- [36] Y. Dovzhenko, F. Casola, S. Schlotter, T. X. Zhou, F. Büttner, R. L. Walsworth, G. S. D. Beach, and A. Yacoby, *Nat. Commun.* **9**, 2712 (2018).
- [37] A. Thiaville, S. Rohart, E. Jué, V. Cros, and A. Fert, *Europhys. Lett.* **100**, 57002 (2012).
- [38] N. S. Kiselev, A. N. Bogdanov, R. Schäfer, and U. K. Rößler, *J. Phys. D: Appl. Phys.* **44**, 392001 (2011).
- [39] W. Legrand, N. Ronceray, N. Reyren, D. Maccariello, V. Cros, and A. Fert, *Phys. Rev. Appl.* **10**, 064042 (2018).
- [40] H.-B. Braun, *Phys. Rev. B* **50**, 16485 (1994).
- [41] C. B. Muratov and V. V. Slastikov, *Proc. R. Soc. London, Ser. A* **473**, 20160666 (2016).
- [42] H. Knüpfer, C. B. Muratov, and F. Nolte, *Arch. Rat. Mech. Anal.* **232**, 727 (2019).
- [43] C. B. Muratov, *Calc. Var. Partial Diff. Eq.* **58**, 52 (2019).
- [44] See Supplemental Material at <http://link.aps.org/supplemental/10.1103/PhysRevB.101.045416> for the derivation of the two-dimensional energy, the minimization among Belavin-Polyakov type profiles, and the proof of existence of minimizers in the considered class, which includes Refs. [63–73].
- [45] A. Bogdanov and A. Hubert, *J. Magn. Magn. Mater.* **138**, 255 (1994).
- [46] J. M. Winter, *Phys. Rev.* **124**, 452 (1961).
- [47] G. Gioia and R. D. James, *Proc. R. Soc. London, Ser. A* **453**, 213 (1997).
- [48] N. Nagaosa and Y. Tokura, *Nat. Nanotechnol.* **8**, 899 (2013).
- [49] H.-B. Braun, *Adv. Phys.* **61**, 1 (2012).
- [50] F. N. Rybakov and N. S. Kiselev, *Phys. Rev. B* **99**, 064437 (2019).
- [51] C. Melcher, *Proc. R. Soc. London, Ser. A* **470**, 20140394 (2014).
- [52] B. Kaplan and G. A. Gehring, *J. Magn. Magn. Mater.* **128**, 111 (1993).
- [53] A. A. Belavin and A. M. Polyakov, *JETP Lett.* **22**, 245 (1975).
- [54] A. Bernard-Mantel, C. B. Muratov, and T. M. Simon, *arXiv:1912.09854*.
- [55] S. Komineas, C. Melcher, and S. Venakides, *arXiv:1904.01408* (unpublished).
- [56] I. Lemesch, F. Büttner, and G. S. D. Beach, *Phys. Rev. B* **95**, 174423 (2017).
- [57] A. Vansteenkiste, J. Leliaert, M. Dvornik, M. Helsen, F. Garcia-Sanchez, and B. Van Waeyenberge, *AIP Adv.* **4**, 107133 (2014).
- [58] A. Bogdanov and A. Hubert, *J. Magn. Magn. Mater.* **195**, 182 (1999).
- [59] A. Bogdanov and A. Hubert, *Phys. Status Solidi (B)* **186**, 527 (1994).
- [60] L. Caretta, L. Mann, F. Büttner, K. Ueda, B. Pfau, C. M. Günther, P. Helsing, A. Churikova, C. Klose, M. Schneider *et al.*, *Nat. Nanotechnol.* **13**, 1154 (2018).
- [61] N. Romming, A. Kubetzka, C. Hanneken, K. von Bergmann, and R. Wiesendanger, *Phys. Rev. Lett.* **114**, 177203 (2015).
- [62] R. Tomasello, E. Martinez, R. Zivieri, L. Torres, M. Carpentieri, and G. Finocchio, *Sci. Rep.* **4**, 6784 (2014).
- [63] F. Hellman, A. Hoffmann, Y. Tserkovnyak, G. S. D. Beach, E. E. Fullerton, C. Leighton, A. H. MacDonald, D. C. Ralph, D. A. Arena, H. A. Durr, P. Fischer, J. Grollier, J. P. Heremans, T. Jungwirth, A. V. Kimel, B. Koopmans, I. N. Krivorotov, S. J. May, A. K. Petford-Long, J. M. Rondinelli, N. Samarth, I. K. Schuller, A. N. Slavin, M. D. Stiles, O. Tchernyshyov, A. Thiaville, and B. L. Zink, *Rev. Mod. Phys.* **89**, 025006 (2017).
- [64] N. A. Usov and O. N. Serebryakova, *J. Appl. Phys.* **121**, 133905 (2017).
- [65] C. B. Muratov, V. V. Slastikov, A. G. Kolesnikov, and O. A. Tretiakov, *Phys. Rev. B* **96**, 134417 (2017).
- [66] R. V. Kohn and V. Slastikov, *Proc. R. Soc. London, Ser. A* **461**, 143 (2005).
- [67] A. Aharoni, *J. Appl. Phys.* **37**, 3271 (1966).

- [68] C. J. García-Cervera, [Euro. J. Appl. Math.](#) **15**, 451 (2004).
- [69] E. H. Lieb and M. Loss, *Analysis* (American Mathematical Society, Providence, RI, 2010).
- [70] R. M. Corless, G. H. Gonnet, D. E. G. Hare, D. J. Jeffrey, and D. E. Knuth, [Adv. Comput. Math.](#) **5**, 329 (1996).
- [71] D. Foster, C. Kind, P. J. Ackerman, J.-S. Tai, B. M. R. Dennis, and I. I. Smalyukh, [Nat. Phys.](#) **15**, 655 (2019).
- [72] L. Döring and C. Melcher, [Calc. Var. Partial Differential Equations](#) **56**, 60 (2017).
- [73] W. Fleming and R. Rishel, [Archiv Math.](#) **11**, 218 (1960).